European Journal of Neuroscience, Vol. 12, pp. 2685–2693, 2000

Single-cell mRNA expression of *HCN1* correlates with a fast gating phenotype of hyperpolarization-activated cyclic nucleotide-gated ion channels (Ih) in central neurons

Oliver Franz,[1,2] Birgit Liss,[1,2] Axel Neu[1,2] and Jochen Roeper[1,2]
[1]Medical Research Council, Anatomical Neuropharmacology Unit, Department of Pharmacology, Oxford University, UK
[2]Centre for Molecular Neurobiology, Hamburg, Germany

Abstract

Hyperpolarization-activated currents (Ih) are key players in shaping rhythmic neuronal activity. Although candidate genes for Ih channels have been cloned (*HCN1–HCN4*), the subunit composition of different native Ih channels is unknown. We used a combined patch-clamp and qualitative single-cell reverse transcription multiplex polymerase chain reaction (RT-mPCR) approach to analyse *HCN1–4* coexpression profiles in four neuronal populations in mouse CNS. Coexpression of *HCN2*, *HCN3* and *HCN4* mRNA was detected in single neurons of all four neuronal cell types analysed. In contrast, *HCN1* mRNA was detected in neocortical and hippocampal pyramidal neurons but not in dopaminergic midbrain and thalamocortical neurons. *HCN1* expression was correlated with significantly faster activation kinetics on the level of individual neurons. Semiquantitative single-cell RT-mPCR analysis demonstrated that *HCN1* mRNA expression is at least eightfold higher in cortical neurons than subcortical neurons. We show that single neurons possess complex coexpression patterns of Ih candidate genes. Alternative expression of *HCN1* is likely to be an important molecular determinant to generate the different neuronal Ih channel species adapted to tune either subcortical or cortical network activity.

Introduction

Hyperpolarization-activated cationic conductances (Ih) are present in many neurons and cardiac cells and are also found in other tissues (DiFrancesco, 1993; Pape, 1994). Ih channels possess small single channel conductances of ~1 pS and are permeable to K^+ and Na^+ ions. They are activated by hyperpolarizations beyond –50 mV and their voltage-dependence is modulated by intracellular cyclic nucleotides. As a consequence of its mixed K^+/Na^+ permeability and inverse voltage-dependence, somatodendritic neuronal Ih channels are involved in several functions (Pape, 1996; Lüthi & McCormick, 1998). The classical function is contributing to a slow pacemaker depolarization after electrical discharge. In addition, Ih will tune the frequency preference and temporal summation of excitatory postsynaptic potentials (EPSPs; Magee, 1999). Thus, Ih channels might act as low-pass filters and help to determine the resonance properties of neurons (Hutcheon *et al*., 1996). Ih currents have also been described in axons (Takigawa *et al*., 1998) and presynaptic terminals (Owens *et al*., 1999).

At least four members of a new family of mammalian Ih candidate genes have been identified (Santoro *et al*., 1997; Ludwig *et al*., 1998; Santoro *et al*., 1998; Ishii *et al*., 1999; Ludwig *et al*., 1999; Seifert *et al*., 1999) and recently a unifying nomenclature has been adopted (Clapham, 1998): *HCN1* (*mBCNG-1, HAC2*); *HCN2* (*mBCNG-2, HAC1*); *HCN3* (*HAC3*); and *HCN4* (*mBCNG-3*). This hyperpolarization-activated, cyclic nucleotide-gated channel family is related to six transmembrane voltage-activated K^+ channels as well as to cyclic nucleotide-gated nonselective channels. Heterologous expression of homomeric *HCN1*, *HCN2* and *HCN4* channels demonstrated that they all possess salient features of native Ih channels (Ludwig *et al*., 1998; Santoro *et al*., 1998; Ludwig *et al*., 1999). However, the role of these genes in the molecular makeup of neuronal Ih channel species is unclear.

The aim of this study was to combine patch-clamp electrophysiology with the single-cell reverse transcription multiplex polymerase chain reaction (RT-mPCR) technique developed by Rossier and coworkers (Lambolez *et al*., 1992; Cauli *et al*., 1997) to determine *HCN1–4* expression profiles on the level of single neurons in different populations characterized by different types of somatodendritic Ih currents. In our study, we analysed dopaminergic midbrain neurons (Mercuri *et al*., 1995) as well as the classical Ih locus, thalamocortical relay neurons (Pape & McCormick, 1989). We also included neocortical layer V and CA1 hippocampal pyramidal cells because they possess Ih currents with different gating properties compared to subcortical neurons (Maccaferri *et al*., 1993; Solomon & Nerbonne, 1993; Budde *et al*., 1994; Magee, 1998).

Materials and methods

Whole-cell recordings and data analysis

Preparation of 250 µm coronal brain slices from mice C57Bl/6J (12–16 postnatal days old killed by cervical dislocation) were performed as previously described (Liss *et al*., 1999). For patch-clamp recordings, slices were transferred to a chamber continuously perfused at 2–4 mL/min with artificial cerebrospinal fluid (ACSF) bubbled with a mixture of 95% O_2/5% CO_2 at room temperature (22–24 °C). Patch pipettes (whole-cell recordings, 1–2.5 MΩ; dendritic recordings, 8–12 MΩ) were pulled from borosilicate glass (GC150TF, Clark, Reading, UK) and filled with internal solution containing (in mM):

Correspondence: Dr J. Roeper, at the Oxford address above.
E-mail: jochen.roeper@pharm.ox.ac.uk

Received 22 October 1999, revised 29 March 2000, accepted 17 April 2000

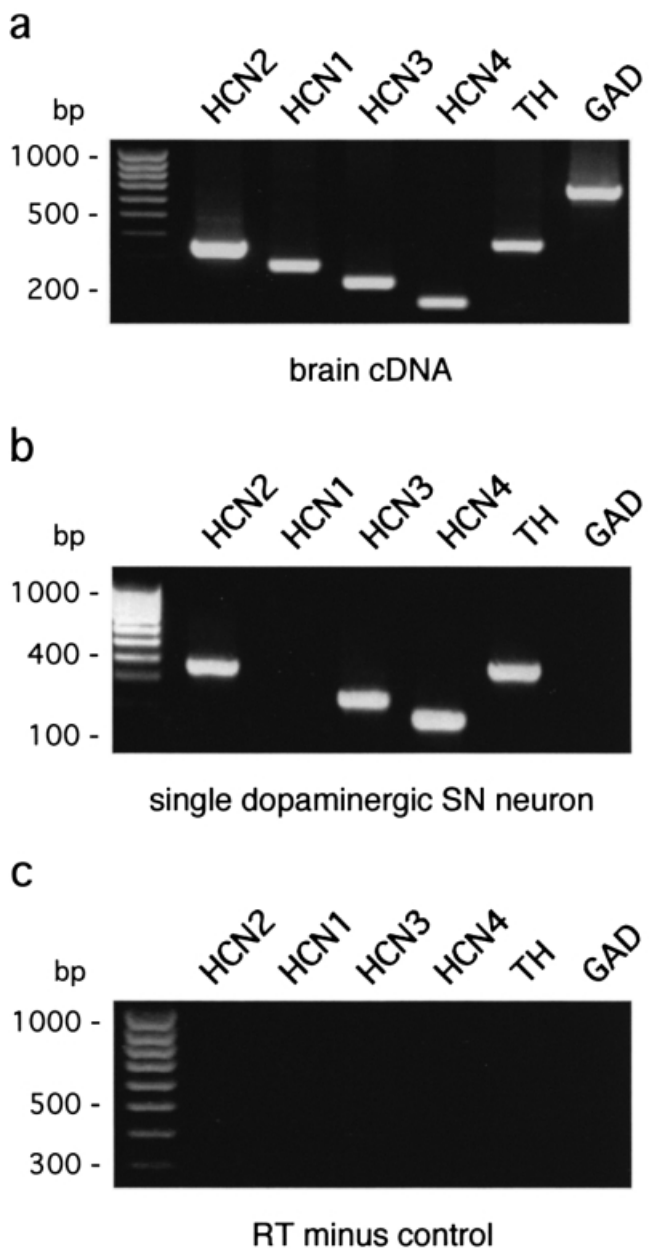

FIG. 1. RT-multiplex PCR (RT-mPCR) of different Ih channel candidate genes. The multiplex protocol was designed to probe for the four putative Ih channel mRNAs HCN1–HCN4 in combination with the marker transcripts tyrosine hydroxylase (*TH*) and glutamate decarboxylase (*GAD67*). The products of the second, nested PCRs were run on a 2% agarose gel in parallel with a 100-bp ladder as molecular weight marker. (a) In mouse whole brain cDNA, all six PCR amplicons could be detected at the size predicted by their mRNA sequences. (b) Result of a RT-mPCR from a single dopaminergic substantia nigra (SN) neuron (single-cell PCR) where *HCN2–4* and *TH* were detected. (c) Result of RT minus control. Without reverse transcriptase in the cDNA reaction, no PCR signal was detected in single-cell material.

KCl, 140; HEPES, 5; EGTA, 5; $MgCl_2$, 3 at pH 7.3. Whole-cell recordings were obtained from somata and dendrites (>50 µm distance from soma) of neurons visualized by infrared differential interference contrast (IR-DIC) videomicroscopy. Recordings were carried out using an EPC-9 patch-clamp amplifier (HEKA Electronic, Lambrecht, Germany). Series resistances were electronically compensated (75–85%). The program package PULSE + PULSEFIT (HEKA Electronic, Lambrecht, Germany) was used for data

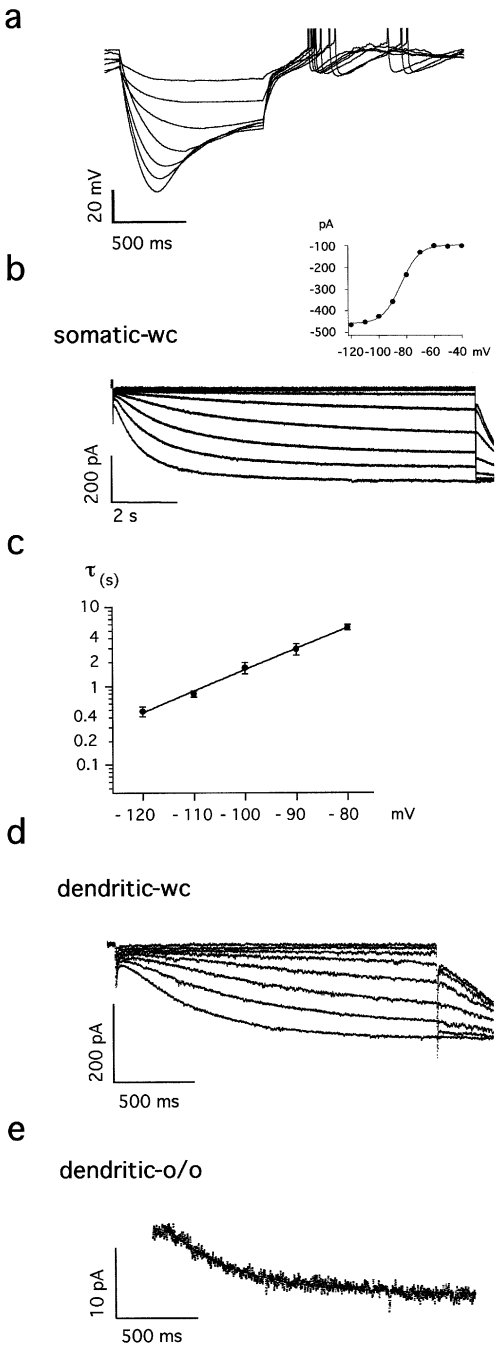

FIG. 2. Slow activating Ih channels in dopaminergic sunbstantia nigra (SN) neurons. (a) Membrane potential responses in a dopaminergic SN neuron to 1 s injections of hyperpolarizing current of increasing amplitudes (20 pA, –80 pA). Note the slow sag component that developed with increasing hyperpolarizations. (b) Somatic whole cell (wc) recordings from dopaminergic SN neurons showed Ih currents with slow activation kinetics in response to 10 s membrane hyperpolarizations from –40 mV to –120 mV in steps of 10 mV from a holding potential of –40 mV followed by a voltage step to –120 mV to record Ih tail currents. Insert shows respective voltage-dependence of Ih activation determined from tail analysis and fitted with a Boltzmann function. (c) Voltage-dependence of mean (● ± SEM; $n = 8$) activation time constants. Line indicates fit by monoexponential function. (d) Dendritic whole cell (wc) recording from a dopaminergic SN neuron showed Ih currents in response to 2 s membrane hyperpolarizations from –40 mV to –120 mV in steps of 10 mV from a holding potential of –40 mV followed by a voltage step to –120 mV (e) Slow activating Ih current in response to a 2-s hyperpolarization to –120 mV from a holding potential of –40 mV in a dendritic outside-out (o/o) recording from a SN neuron overlaid with a fitted monoexponential function with a time constant of tau-1 = 518 ms.

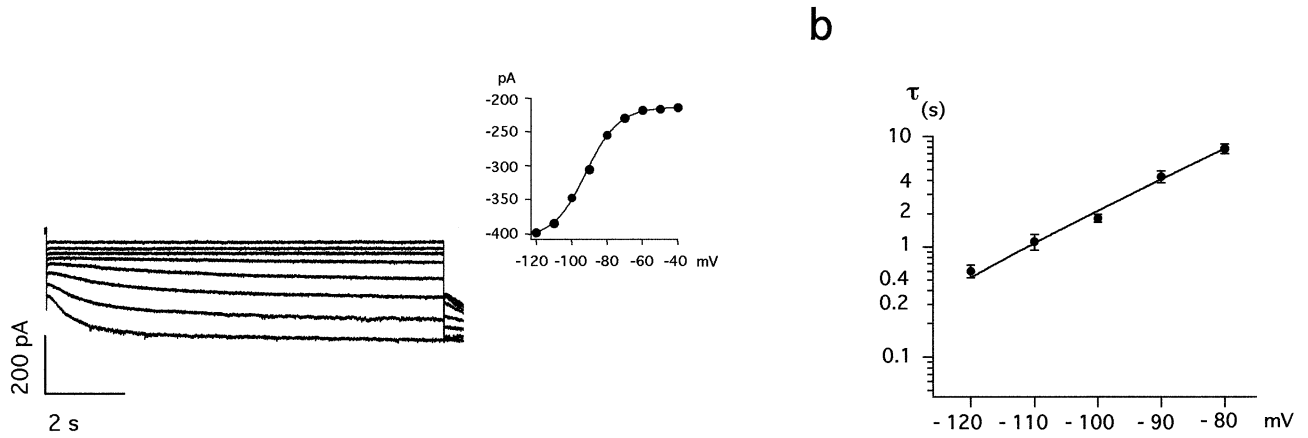

FIG. 3. Slow activating Ih channels in thalamocortical neurons. (a) Somatic whole-cell recordings from thalamocortical relay neuron showed Ih currents with slow activation kinetics in response to 10 s membrane hyperpolarizations from –40 mV to –120 mV in steps of 10 mV from a holding potential of –40 mV followed by a voltage step to –120 mV to record Ih tail currents. Insert shows respective voltage-dependence of Ih activation determined from tail analysis and fitted with a Boltzmann function. (b) Voltage-dependence of mean (● ± SEM, $n = 8$) activation time constants. Line indicates fit by monoexponential function.

acquisition and analysis. Recordings were digitized at 2–5 kHz and filtered with low-pass filter Bessel characteristics of 0.4–1 kHz cut-off frequency. The time constants of activation were fitted with no constraints to both mono- and biexponential equations {f*exp[–x/(tau-1)] + s*exp[–x/(tau-2)]} using a nonlinear least-square fitting routine (Levenberg–Marquardt algorithm) in IGOR (Wavemetrics, USA). The goodness-of-fit was analysed by computing the residuals and quantified by comparing the χ^2 values and the standard deviation of the parameters. Significance levels were determined by Student's *t*-test. Data are given as mean ± SEM. Ignoring the sigmoidal onset of Ih activation (Pape, 1996), mono- and biexponential functions were chosen to facilitate direct comparison with heterologously expressed HCN channels (Santoro *et al*., 1998; Ludwig *et al*., 1999; Seifert *et al*., 1999).

Multiplex and nested PCR

Harvesting of cytoplasm and reverse transcription were carried out as previously described (Liss *et al*., 1999). Following reverse transcription, the cDNAs for *HCN1–4*, for tyrosine hydroxlase (TH) and the 67 kDa form of glutamate decarboxylase (GAD67) were simultaneously amplified in a multiplex PCR using the following set of primers (from 5′ to 3′): *HCN1* (*HAC2*, accession No. AJ225123) sense, TCTTGCGGTTATTACGCCTT (position 985), antisense, TTTTCTTGCCTATCCGATCG (position 1983); *HCN2* (*HAC1*, accession No. AJ225122) sense, TACTTGCGTACGTGGTTCGT (position 810), antisense, GAAATAGGAGCCATCCGACA (position 1775); *HCN3* (*HAC3*, accession No. AJ225124) sense, CGCATCCACGAGTACTACGA (position 1242), antisense, CACTTCCAGAGCCTTTACGC (position 2322); *HCN4* (*mBCNG-3*, accession No. AF064874) sense, TCTGATCATCATACCCGTGG (position 295), antisense, GAAGACCTCGAAACGCAACT (position 1315); TH (accession No. M69200) sense, CACCTGGAGTACTTTGTGCG (position 387), antisense, CCTGTGGGTGGTACCCTATG (position 1525); GAD67 (accession No. Z49976) sense, TGACATCGACTGCCAATACC (position 731), antisense, GGGTTAGAGATGACCATCCG (position 1835). Multiplex and nested PCR were performed as previously described (Liss *et al*., 1999). Nested PCR amplifications were carried out using the following primer pairs: *HCN1* sense, CTCTTTTTGCTAACGCCGAT (position 1612), antisense, CATTGAAA-TTGTCCACCGAA (position 1902); *HCN2* sense, GTGGAGCGAGCTCTACTCGT (position 1181), antisense, GTTCACAATCTCCTCACGCA (position 1550); *HCN3* sense, GCAGCATTTGGTACAACACG (position 1808), antisense, AGCGTCTA-GCAGATCGAGCT (position 2040); *HCN4* sense, GACAGCGCATCCATGACTAC (position 1110), antisense, ACAAAGTTGGGATCTGCGTT (position 1278); TH sense, TGCACACAGTACATCCGTCA (position 936), antisense TCTGACAC-GAAGTACACCGG (position 1312); GAD67 sense, CATATGAAATTGCACCCGTG (position 761), antisense, CGGTGTCATAGGAGACGTCA (position 1462). The PCR products (15 µL aliquots) were separated and visualized in an ethidium bromide-stained agarose gel (2%) by electrophoresis. The predicted sizes (bp) of the PCR-generated fragments were: 702 (GAD67); 377 (TH); 370 (*HCN2*); 291 (*HCN1*); 233 (*HCN3*); and 169 (*HCN4*). All individual PCR products were verified by direct sequencing. RNA isolation and cDNA preparation for control reactions was carried out as described previously (Liss *et al*., 1999). All six PCR fragments were detected routinely in the positive control with the PCR protocol described above. Negative controls, where patch pipettes were filled with the single-cell PCR solution, advanced into the slice preparation without harvesting single-cell material, expelled and subjected to the RT-mPCR protocol, were also carried out in parallel to all single-cell experiments. In addition, single-cell mPCR amplifications were carried out without prior reverse transcription to probe for possible amplification of genomic DNA from the harvested single nuclei (RT minus control). For semiquantitative single-cell RT-PCR of HCN1 we generated serial dilutions (1/2, 1/4, 1/8, 1/16, 1/32, 1/64) of single-cell cDNA pools. Each dilution was used as template in a nested PCR (2×35 cycles) with *HCN1* primers as described above. Detection thresholds were analysed using agarose gel electrophoresis.

Results

Single-cell RT-mPCR for Ih candidate genes

An RT-mPCR protocol was designed to simultaneously detect, at the single-cell level in mouse brain slices, the mRNAs of the putative Ih channel subunits HCN1 (BCNG-1, HAC2), HCN2 (BCNG-2, HAC1), HCN3 (BCNG-4, HAC3), and HCN4 (BCNG-3). In addition, the protocol probed for the expression of the marker genes *TH* for dopaminergic neurons and *GAD67* for GABAergic neurons. Figure 1a shows that six specific PCR products were detected from whole brain cDNA diluted to the picogram range. The size of each of the PCR

amplicons was predicted by its respective mRNA sequence. Consistent with previous findings, all mRNAs for the four Ih channel subunits are expressed in brain as well as *TH* and *GAD67*. The established single-cell RT-mPCR protocol was then used to analyse Ih channel subunit expression in several neuronal cell types, e.g. dopaminergic substantia nigra (SN) neurons (Fig. 1b). As the genomic structures of the *HCN* genes were unknown at the time of primer design, single-cell mPCR amplifications were carried out without prior reverse transcription to probe for possible amplification of genomic DNA from the harvested single nuclei (RT minus control). For all analysed neurons ($n = 10$) no PCR products were detectable (Fig. 1c). Thus, our protocol was suited to study genuine *HCN* mRNA expression profiles of single neurons.

Fast and slow activating somatodendritic Ih channels in central mouse neurons

In previous studies, large amplitude, slow activating Ih currents were described in dopaminergic SN neurons (Mercuri *et al.*, 1995) and thalamic relay neurons in rat and other species (Pape, 1996). As evident from their slow sag components in response to hyperpolarizing currents (Fig. 2a) mouse dopaminergic SN neurons also displayed significant Ih conductances. We characterized Ih properties in the standard whole-cell configuration in the presence of 500 nM tetrodotoxin, 50 μM picrotoxin and 10 μM DNQX to block sodium channels and fast synaptic transmission. Slow activating Ih currents were elicited by 2–20 s membrane hyperpolarizations of increasing amplitude followed by a voltage step to –120 mV to analyse Ih tail currents (Fig. 2b). The tail currents were used to analyse the voltage dependence of Ih in dopaminergic SN neurons. As previously observed (Seifert *et al.*, 1999), half-maximal activation of Ih critically depends on pulse duration. With 2 s voltage steps, the mean half-maximal activation (V_{50}) of Ih was -89.2 ± 1.1 mV and the mean slope was 9.6 ± 0.4 mV ($n = 13$). Using 10 s voltage steps (Fig. 2b), the mean V_{50} was more positive at -82.9 ± 1.0 mV and the mean slope was 6.5 ± 0.3 mV ($n = 8$). Further increase of the duration of the hyperpolarizing voltage step to 20 s gave very similar results ($V_{50} = -81.3 \pm 1.2$ mV, slope $= 6.7 \pm 0.3$ mV; $n = 4$) indicating a saturation of the pulse-length-dependent shift of V_{50}. The time course of Ih activation during 10 s hyperpolarizing voltage steps was best described by double-exponential functions. In the voltage range between –80 mV and –120 mV the dominant component of Ih activated with time constants ranging between 5 s and 500 ms in dopaminergic SN neurons (Fig. 2c). Close to full activation, the mean time constant of the dominant faster component was tau-1 (@ –120 mV) $= 482 \pm 70$ ms ($n = 8$) and that of the slower one was tau-2 @ –120 mV $= 2.09 \pm 0.42$ s ($n = 8$). Similar time constants were

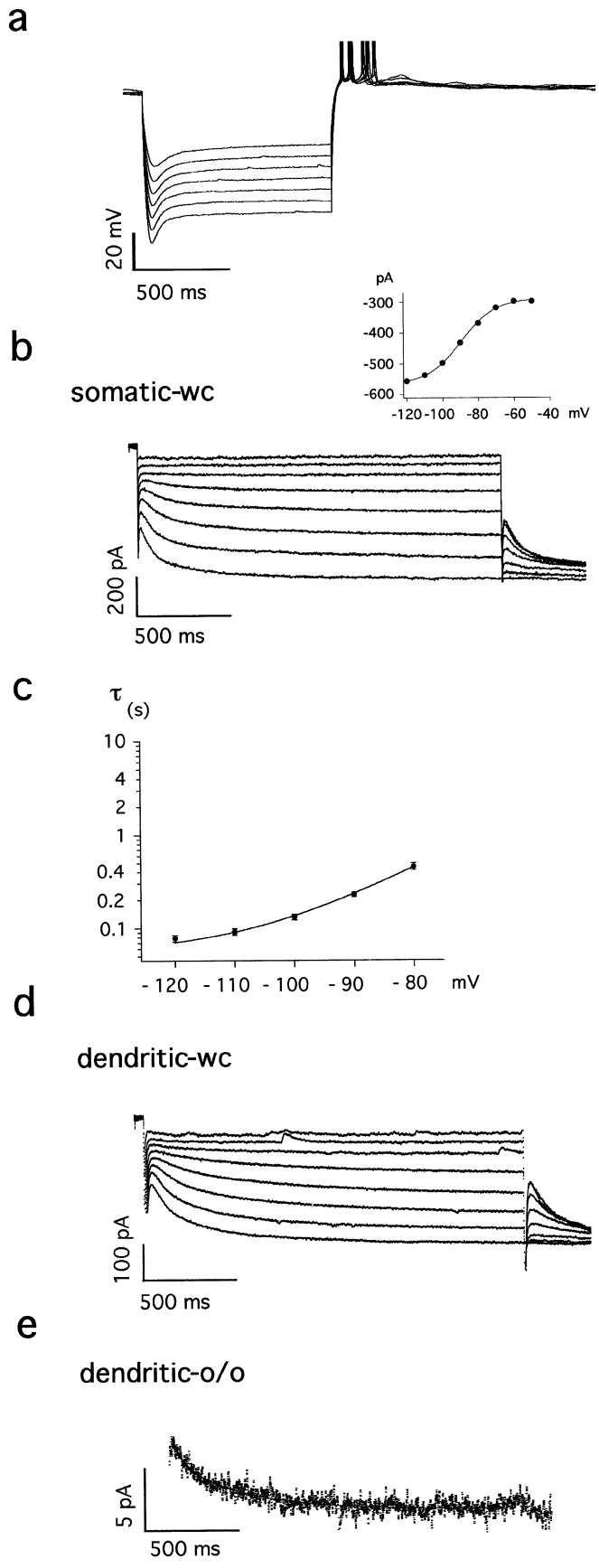

FIG. 4. Fast activating Ih channels in neocortical layer V neurons. (a) Membrane potential responses in a neocortical layer V neuron to 1 s injections of hyperpolarizing current of increasing amplitudes (20 pA, –80 pA). Note the fast sag component. (b) Somatic whole cell (wc) recording from a neocortical layer V neuron demonstrated Ih currents with fast activation kinetics in response to 2 s membrane hyperpolarizations from –50 mV to –120 mV in steps of 10 mV from a holding potential of –40 mV followed by a voltage step to –120 mV to record Ih tail currents. Insert shows respective voltage-dependency of Ih activation fitted with a Boltzmann function. (c) Voltage-dependence of mean τ (± SEM, $n = 8$) activation time constants. Line indicates fit by monoexponential function. (d) Dendritic whole cell (wc) recording from a neocortical layer V neuron demonstrated Ih currents with a fast activation. Voltage protocol as in (b). (e) Ih current with fast activating component in response to a 2-s membrane hyperpolarization to –120 mV in a dendritic outside-out (o/o) recording from a neocortical layer V neuron overlaid with a fitted biexponential function with tau-1 = 63 ms and tau-2 = 420 ms.

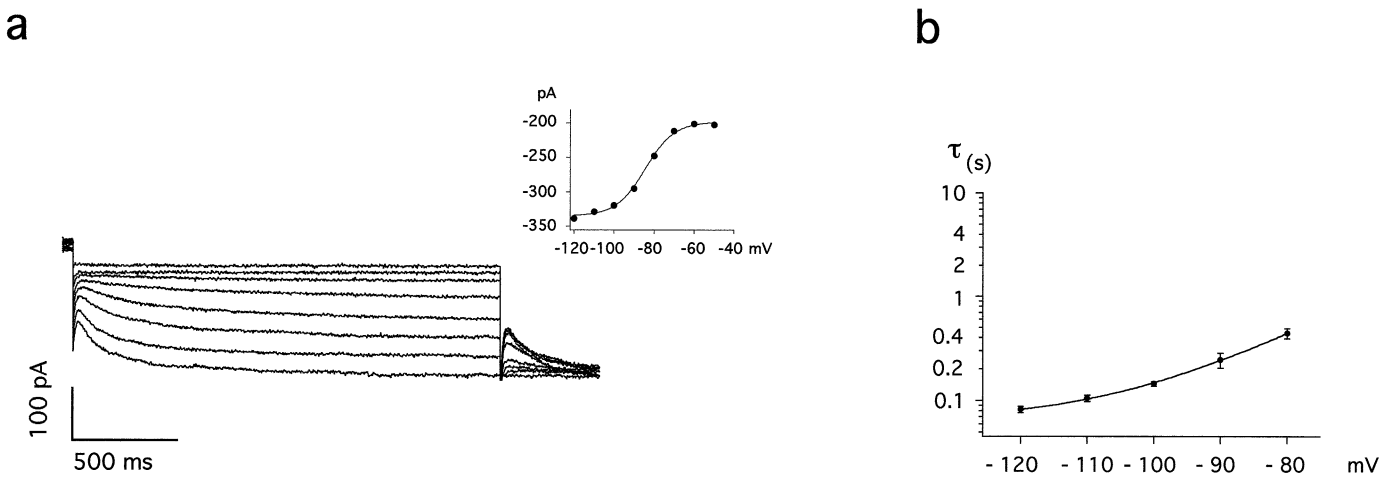

FIG. 5. Fast activating Ih channels in hippocampal CA1 neurons. (a) Somatic whole-cell (wc) recordings from hippocampal CA1 neurons showed Ih currents with fast activation kinetics in response to 2 s membrane hyperpolarizations from –50 mV to –120 mV in steps of 10 mV from a holding potential of –40 mV followed by a voltage step to –120 mV to record Ih tail currents. Insert shows respective voltage-dependence of Ih activation determined from tail analysis and fitted with a Boltzmann function. (b) Voltage-dependence of mean (± SEM, $n = 8$) activation time constants. Line indicates fit by monoexponential function.

obtained from analysis of Ih activation elicited with shorter (2 s) hyperpolarizing voltage steps (tau-1 (@ –120 mV) = 387 ± 42 ms, tau-2 (@ –120 mV) = 1.82 ± 0.33 ms; $n = 29$).

The inclusion of 1 mM 8-Bromo-cAMP in the pipette solution induced a positive voltage shift of 11 mV to a mean half-activation voltage of –78.7 ± 1.1 mV (2 s voltage-steps) without significant changes in the slope of the activation curve (9.6 ± 0.6 mV, $n = 6$). Ih currents were not detectable in large (nucleated) outside-out patches from dopaminergic SN neurons (not shown) which indicated that Ih channels are preferentially expressed in dendritic compartments. Indeed large Ih currents were observed in dendritic whole-cell recordings (Fig. 2d) and Ih channels were also present in dendritic outside-out recordings (Fig. 2e) from dopaminergic SN neurons. Although differences in series resistances and cable properties in the dendritic tree are expected to affect the results, the comparison of the voltage-dependencies in somatic and dendritic whole-cell recordings revealed no significant differences (2 s voltage-steps: dendritic whole-cell V_{50} = –87.0 ± 0.6 mV, slope = 8.1 ± 0.6 mV, $n = 7$). In contrast to somatic recordings, the kinetics of Ih activation in dendritic recordings were best described by monoexponential functions with time constants similar to the fast component in somatic recordings (dendritic whole cell tau-1 (@ –120 mV) = 497 ± 27 ms, $n = 7$; dendritic outside-out tau-1 (@ –120 mV) = 542 ± 22 ms, $n = 5$).

For comparison, we also studied the properties of Ih currents in thalamocortical relay neurons. As shown in Fig. 3, activation kinetics and voltage dependence of Ih in this neuronal population were similar to those obtained in dopaminergic SN neurons and a similar pulse-length dependent shift of V_{50} was observed [V_{50} (2 s voltage steps) = –90.9 ± 1.2 mV, slope = 8.7 ± 0.5, $n = 11$; V_{50} (10 s voltage steps) = –90.5 ± 0.8 mV, slope = 6.6 ± 0.8, $n = 6$; V_{50} (20 s voltage steps) = –83.1 ± 1.8 mV, slope = 7.1 ± 0.6, $n = 4$]. Also for thalamocortical neurons, the time course of Ih activation during 10 s hyperpolarizing voltage steps (Fig. 3a) was best described by double-exponential functions. In the voltage range between –80 mV and –120 mV the dominant component of Ih activated with time constants ranging between 7.5 s and 600 ms in thalamocortical neurons (Fig. 3b). Close to full activation, the mean time constant of the dominant faster component was tau-1 (@ –120 mV) = 602 ± 80 ms ($n = 8$) and that of the slower one was tau-2 (@ –120 mV) = 2.70 ± 0.56 s, $n = 8$). Similar time constants were obtained from analysis of thalamocortical Ih activation elicited by shorter, 2 s hyperpolarizing voltage steps (tau-1 (@ –120 mV) = 445 ± 25 ms, tau-2 (@ –120 mV) = 2.53 ± 0.36 ms, $n = 20$). The ratios between the amplitudes of the dominant fast (tau-1) and the slow (tau-2) components (Rtau1/2) were also similar in dopaminergic SN neurons (Rtau1/2 (@ –120 mV) = 2.8 ± 0.6, $n = 8$) and thalamocortical neurons (Rtau1/2(@ –120 mV) = 2.6 ± 0.3, $n = 8$).

Analysis of the functional properties of Ih currents both in neocortical layer V and hippocampal CA1 neurons suggested that these pyramidal cells possess a different, significantly faster activating Ih species (Figs 4 and 5). This was already evident from comparing the kinetics of the sag component in response to hyperpolarizing current injections in cortical (Fig. 4a) vs. subcortical neurons (Fig. 2a). The voltage-dependence of cortical and hippocampal Ih determined with 2 s voltage steps was very similar, with mean half-maximal activation voltages at –83.3 ± 1.1 mV (cortex, $n = 14$) and –84.3 ± 0.5 mV (hippocampus, $n = 15$) and mean slopes of 9.8 ± 0.5 mV (cortex, $n = 14$) and 10.1 ± 0.3 mV (hippocampus, $n = 15$), respectively. Also in these neurons, the time course of Ih activation in response to hyperpolarizing voltage steps was best described by double-exponential functions with a dominant faster component that had time constants ranging between 50 and 500 ms in the voltage range between –80 mV and –120 mV (Figs 4c and 5b). The minor slow component had time constants in the order of 500–700 ms (cortex tau-1 (@ –120 mV) = 84.1 ± 4.6 ms, tau-2 (@ –120 mV) = 660 ± 81 ms, $n = 19$; hippocampus tau-1 (@ –120 mV) = 64.4 ± 2.9 ms, tau-2 (@ –120 mV) = 537 ± 47 ms, $n = 18$). The ratios between the amplitudes of the fast (tau-1) and the slow (tau-2) components (Rtau1/2) were also very similar in cortical (Rtau1/2 (@ –120 mV) = 1.5 ± 0.1, $n = 19$) and hippocampal pyramidal neurons (Rtau1/2(@ –120 mV) = 1.6 ± 0.1, $n = 18$).

The effect of cyclic nucleotides on this Ih species was smaller compared to that of subcortical neurons. In hippocampal CA1 neurons, inclusion of 1 mM 8-Bromo-cAMP in the pipette solution only induced a positive shift of 7 mV to a half-maximal activation voltage of –77.4 ± 2.5 mV ($n = 5$). Similar to subcortical neurons, Ih channels in hippocampal CA1 were shown to be preferentially expressed in dendritic compartments (Magee, 1998). This was also the case for neocortical layer V neurons where Ih currents were detected in dendritic whole-cell and dendritic outside-out recordings

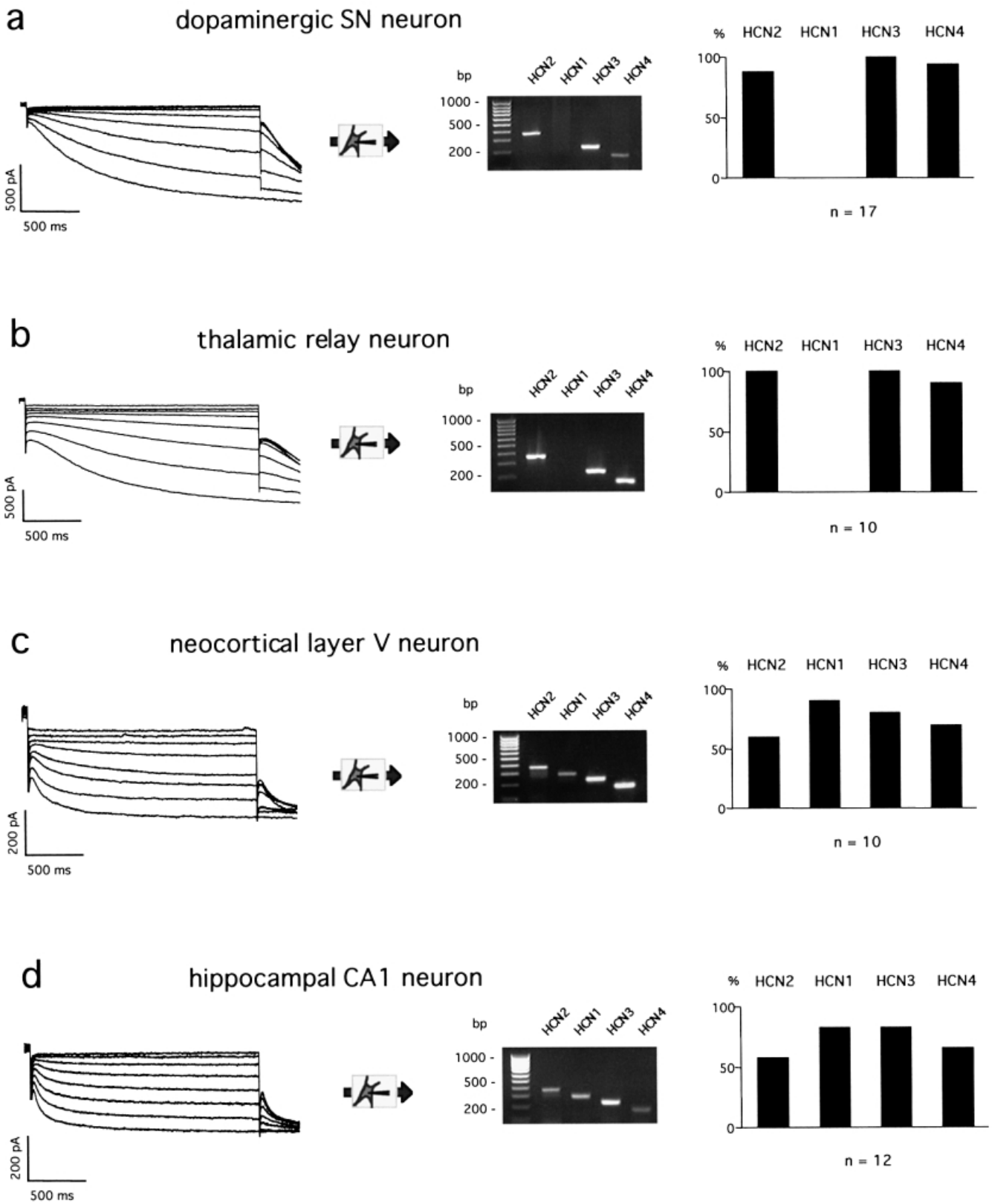

FIG. 6. Qualitative single-cell RT-mPCR expression profiles of HCN1–4 mRNAs in four neuronal populations. (a–e) Left panels show current responses to 2 s membrane hyperpolarizations from –50 mV to –120 mV in steps of 10 mV from a holding potential of –40 mV followed by a voltage step to –120 mV from different neuronal cell types as indicated. After electrophysiological analysis, cytoplasm of the cells was harvested for single-cell RT-mPCR. Middle panels show the respective agarose gel analyses of *HCN1–4* expression profiles in these cells. Marker transcripts are not shown. Right panels show the detection (in percentage) of the different HCN transcripts by single-cell PCR in the respective neuronal populations.

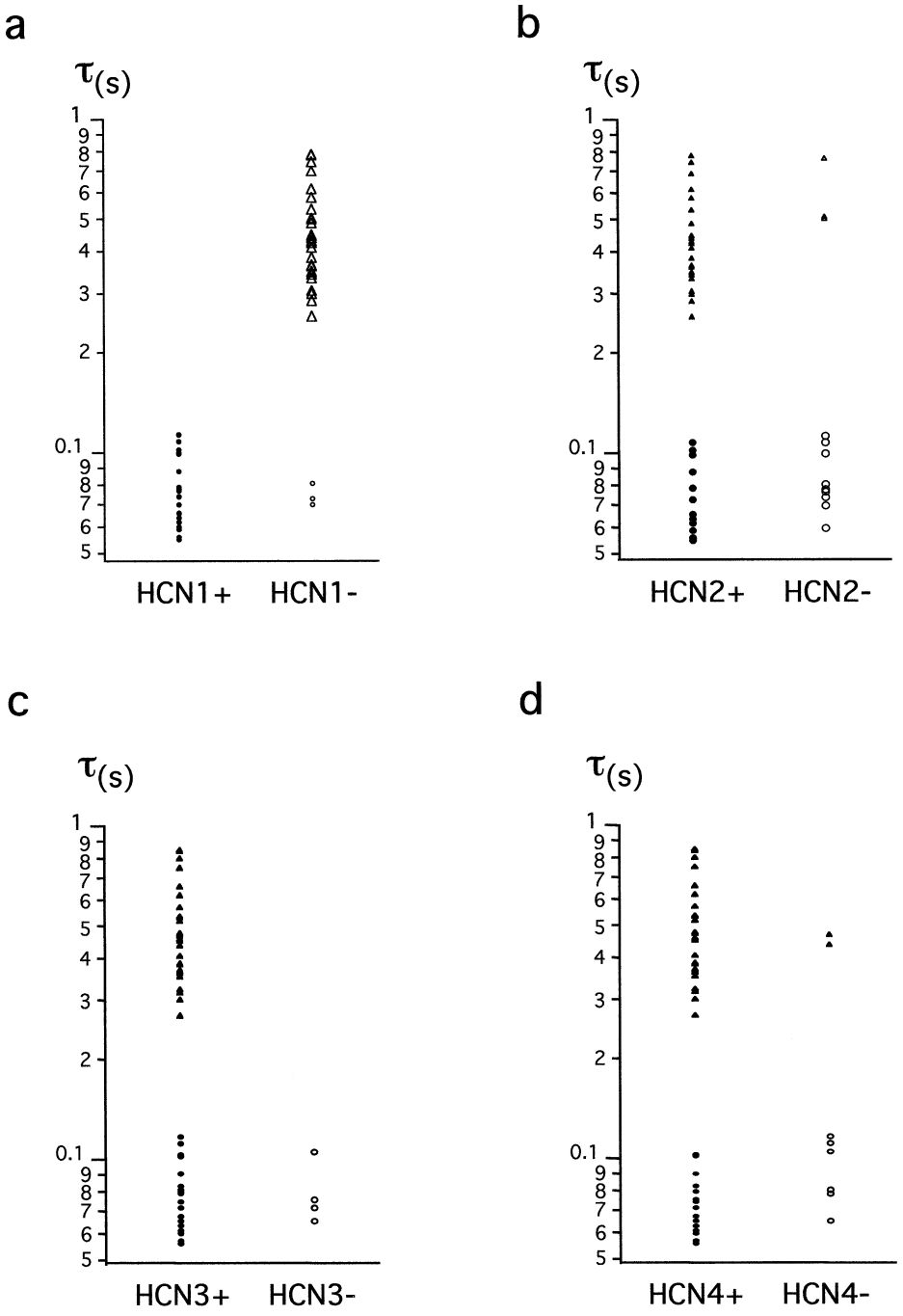

FIG. 7. Single-cell genotype/phenotype correlations between detection and nondetection of *HCN1–4* subunits and time constants of Ih activation. (a–d) Single-cell genotype/phenotype correlations. Time constants of Ih activation (dominant component (@ –120 mV)) are plotted against detection (● cortical neurons, ▲ subcortical neurons) or nondetection (™ cortical neurons, ○ subcortical neurons) of HCN1–4 mRNAs in the same cells.

(Fig. 4de). The voltage-dependence and activation kinetics of Ih currents obtained from dendritic recordings in cortical layer V cells were similar to those of somatic recordings (dendritic whole-cell $V_{50} = -78.9 \pm 0.8$ mV, slope = 6.8 ± 0.8 mV; tau-1 (@ –120 mV) = 82.7 ± 10.0 ms, tau-2 (@ –120 mV) = 417 ± 83 ms, $n = 6$; dendritic outside-out tau-1 (@ –120 mV) = 65.0 ± 5.3 ms, tau-2 (@ –120 mV) = 449 ± 31 ms $n = 4$).

Alternative coexpression of HCN subunits correlates with different Ih phenotypes in central neurons

Figure 6 summarizes the results of our single-cell RT-mPCR study for all four neuronal populations analysed. The left panels show current responses to 2 s membrane hyperpolarizations of increasing amplitudes followed by a voltage step to –120 mV. The middle panels depict the respective agarose gel analyses of the *HCN1–4* expression profiles for the same cells. The right panels give the relative percentage of detection of all HCN mRNAs probed in the respective cell populations. Both subcortical cell types, dopaminergic SN ($n = 17$, *GAD67*$^-$ *TH*$^+$ and thalamic relay neurons ($n = 10$; *GAD67*$^-$ *TH*$^-$) not only displayed very similar Ih phenotypes but also identical *HCN2–4* coexpression profiles while *HCN1* was not detected (Fig. 4a and b). In contrast, neocortical layer V pyramidal neurons ($n = 10$; *GAD67*$^-$ *TH*$^-$) and hippocampal CA1 neurons ($n = 12$; *GAD67*$^-$ *TH*$^-$), which both possessed a fast activating Ih subtype, displayed *HCN1* expression in addition to *HCN2–4* (Fig. 6c and d). Figure 7 plots single-cell genotype/phenotype correlations for *HCN1–4* comparing the expres-

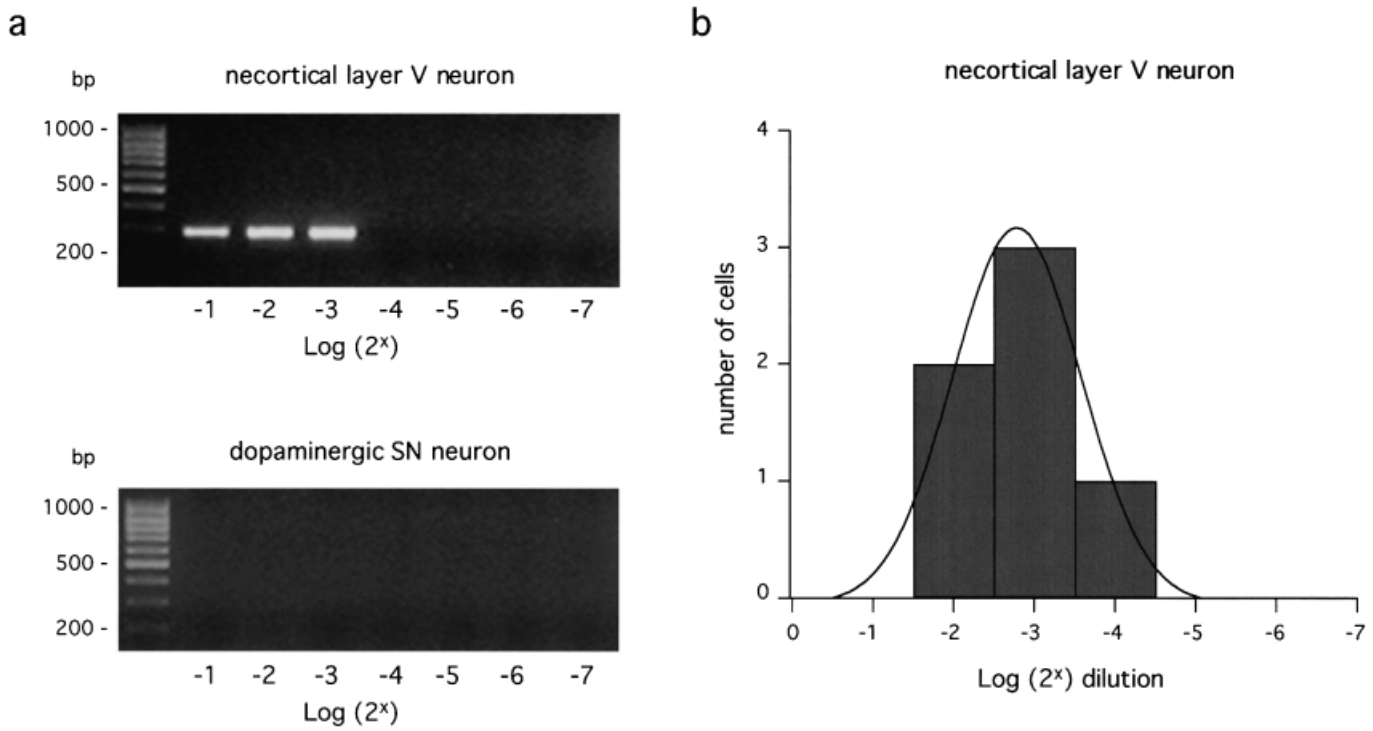

FIG. 8. Semiquantitative single-cell RT-nested PCR for HCN1 mRNA: serial dilutions of single-cell cDNA pools. (a) Representative results of serial dilution experiments (1/2, 1/4, 1/8, 1/16, 1/32, 1/64, 1/256) of single-cell cDNA pools. The products of the second, nested PCRs for each serial dilution step from single-cell cDNA pools of neocortical layer V neurons (upper panel) and dopaminergic substantia nigra (SN) neurons (lower panel) were run on a 2% agarose gel in parallel with a 100-bp ladder as molecular weight. *HCN1* was not detected in serial dilutions of dopaminergic SN neurons ($n = 7$). (b) Frequency distribution of *HCN1* detection thresholds in neocortical layer V neurons fitted with a Gaussian function indicating a mean detection of *HCN1* from 13% ($2^{-2.87}$) of the single-cell cDNA pool ($n = 6$).

sion of *HCN1–4* in a given neuron with the time constant of activation determined in the same cell. Only for *HCN1* did we detect a clear correlation between HCN1 mRNA and a fast gating phenotype and the absence of a HCN1 signal and a slow gating phenotype (Fig. 7a).

In addition to these qualitative single-cell PCR results, we used serial dilutions of single-cell cDNA pools as previously described by Surmeier and coworkers (Tkatch *et al.*, 1998, 2000) to quantify the PCR detection limits of HCN1 mRNA in single neocortical layer V neurons (Fig. 8a). The frequency distribution of single-cell *HCN1* detection thresholds in neocortical neurons was well described with a Gaussian function, indicating a mean *HCN1* detection threshold from approximately 13% (about 1/8) of the single cell cDNA pools (Fig. 8b). In contrast, HCN1 mRNA was neither detected in similar serial dilution single-cell RT-PCR experiments of dopaminergic SN neurons ($n = 7$; Fig. 8a) nor in our qualitative RT-mPCR experiments of subcortical neurons ($n = 27$; Fig. 6). These results indicate that HCN1 mRNA is expressed with at least an eightfold higher abundance in neocortical pyramidal neurons compared to dopaminergic SN neurons. In summary, our results show that single-cell expression of *HCN1* is strongly correlated with a fast Ih gating phenotype in central neurons (SN $HCN1^-$ tau-1 (@ –120 mV) = 435 ± 45 ms, $n = 17$; thalamus $HCN1^-$ tau-1(@ –120 mV) = 409 ± 23 ms, $n = 10$; hippocampus $HCN1^+$ tau-1 (@ –120 mV) = 78.0 ± 6.2 ms, $n = 10$; cortex $HCN1^+$ tau-1 (@ –120 mV) = 81.8 ± 5.9 ms).

Discussion

We have determined the single-cell mRNA coexpression profiles of Ih candidate genes *HCN1–4* in four different neuronal populations. We discovered a strong single-cell correlation between the presence of a fast activating Ih current with time constants < 100 ms and the detection of HCN1 mRNA. In contrast to HCN1 mRNA, which was detected only in hippocampal and neocortical neurons, HCN2–4 mRNAs were coexpressed in both cortical and subcortical neurons. Also, *HCN2–4* detection was not correlated with neither the fast cortical nor the slow subcortical Ih gating phenotype. To further characterize the qualitative differences in *HCN1* expression revealed by the single-cell RT-multiplex PCR, we applied a semiquantitative single-cell RT-PCR protocol based on serial dilutions of single-cell cDNA pools. Assuming comparable reverse transcription efficiencies in different cell types, the semiquantitative protocol compares relative expression levels of mRNA species by determining their single-cell detection thresholds (Tkatch *et al.*, 1998, 2000). We did not detect *HCN1* in serial dilutions of dopaminergic SN neurons. In comparison, the mean *HCN1* detection threshold was about 1/8 of the single-cell cDNA pool in neocortical neurons. This indicates that the abundance of HCN1 mRNA is at least eightfold higher in neocortical compared to dopaminergic SN neurons.

Our results suggests that differential expression of *HCN1* subunits might be an important mechanism in the generation of functional diversity of neuronal Ih channels. Our findings are consistent with the properties of heterologously expressed HCN species. HCN1 channels possess time constants < 100 ms, while HCN2 channels have time constants in the range of 200–400 ms (Santoro *et al.*, 1998; Ludwig *et al.*, 1999). HCN3, as well as HCN4, channels activate even slower with time constants ranging from 400 ms to several seconds (Jegla *et al.*, 1999; Seifert *et al.*, 1999). The immunocytochemical localization of HCN1 protein in dendrites of pyramidal neurons

(Santoro *et al*., 1997) further supports its proposed role as a key subunit in cortical and hippocampal neurons. In addition, recombinant HCN1 channels possess a smaller cAMP sensitivity compared to HCN2 and HCN4 (Clapham, 1998; Seifert *et al*., 1999), which is also consistent with our observation of smaller cAMP sensitivities of native Ih channels in hippocampal neurons compared to those in SN neurons.

In contrast to fast gating Ih currents, our qualitative single-cell RT-multiplex study did not identify a correlation between qualitative detection of a single HCN subtype and the slow activating subcortical Ih phenotype. *HCN2*, *HCN3*, and *HCN4* were coexpressed in most dopaminergic and thalamic neurons. Recent *in situ* hybridization studies might indicate a prominent role for *HCN4* in the generation of subcortical Ih channels (Moosmang *et al*., 1999; Seifert *et al*., 1999). However, our current knowledge about native HCN channel complexes is limited. The functional stoichiometry, the degree of heteromerization, and subcellular targeting of native HCN channel complexes *in vivo* is completely unknown. Our results present the first evidence that alternative coexpression of HCN mRNAs does occur on the level of single neurons and might be involved in the generation of different types of somatodendritic Ih channels. These molecular differences are likely to have important functional consequences which could help to establish the different frequency preferences of postsynaptic computation between cortical and subcortical neurons (Connors & Amitai, 1997; Lüthi & McCormick, 1998; Steriade, 1998).

Acknowledgements

This work was supported by grants of the Deutsche Forschungsgemeinschaft (SFB1630, projekt A4) and the Medical Research Council to J.R. We thank R. Veh (Charité, Berlin) and U. Beisiegel (Hamburg University) for generous support. B.L. is a Blaschko Visiting Research Fellow at Linacre College, Oxford. J.R. holds the Monsanto Senior Research Fellowship at Exeter College, Oxford.

Abbreviations

GAD, glutamate decarboxylase; RT-mPCR, reverse transcription multiplex polymerase chain reaction; SN, substantia nigra; TH, tyrosine hydroxylase, wc, whole-cell.

References

Budde, T., White, J.A. & Kay, A.R. (1994) Hyperpolarization-activated Na (+) -K+ current (Ih) in neocortical neurons is blocked by external proteolysis and internal TEA. *J. Neurophysiol.*, **72**, 2737–2742.

Clapham, D.E. (1998). Not so funny anymore: pacing channels are cloned. *Neuron*, **21**, 5–7.

Cauli, B., Audinat, E., Lambolez, B., Angulo. M.C., Ropert, N., Tsuzuki, K., Hestrin, S. & Rossier, J. (1997) Molecular and physiological diversity of cortical nonpyramidal cells. *J. Neurosci.*, **17**, 3894–3906.

Connors, B.W. & Amitai, Y. (1997) Making waves in the neocortex. *Neuron*, **18**, 347–349.

DiFrancesco, D. (1993) Pacemaker mechanisms in cardiac tissue. *Annu. Rev. Physiol.*, **55**, 455–472.

Hutcheon, B., Miura, R.M. & Puil, E. (1996) Models of subthreshold membrane resonance in neocortical neurons. *J. Neurophysiol.*, **76**, 698–714.

Ishii, T.M., Takano, M., Xie, L.H., Noma, A. & Ohmori, H. (1999) Molecular characterization of the hyperpolarization-activated cation channel in rabbit heart sinoatrial node. *J. Biol. Chem.*, **274**, 12835–12839.

Jegla, T., Bachmann, J., Silvia, C., Stocker, J. & Wagoner, P.K. (1999) Cloning and expression of a novel hyperpolarization-activated cation channel, human HCN3. *Soc. Neurosci. Abstr.*, **25**, 893.6.

Lambolez, B., Audinat, E., Bochet, P., Crepel, F. & Rossier, J. (1992) AMPA receptor subunits expressed by single purkinje cells. *Neuron*, **9**, 247–258.

Liss, B., Bruns, R. & Roeper, J. (1999) Alternative sulfonylurea receptor expression defines metabolic sensitivity of K-ATP channels in dopaminergic midbrain neurons. *EMBO J.*, **18**, 833–846.

Ludwig, A., Zong, X., Jeglitsch, M., Hofmann, F. & Biel, M. (1998) A family of hyperpolarization-activated mammalian cation channels. *Nature*, **393**, 587–591.

Ludwig, A., Zong, X., Stieber, J., Hullin, R., Hofmann, F. & Biel, M. (1999) Two pacemaker channels from human heart with profoundly different activation kinetics. *EMBO J.*, **18**, 2323–2329.

Lüthi, A. & McCormick, D.A. (1998). H-current: properties of a neuronal and network pacemaker. *Neuron*, **21**, 9–12.

Maccaferri, G., Mangoni, M., Lazzari, A. & DiFrancesco, D. (1993) Properties of the hyperpolarization-activated current in rat hippocampal CA1 pyramidal cells. *J. Neurophysiol.*, **69**, 2129–2136.

Magee, J.C. (1998) Dendritic hyperpolarization-activated currents modify the integrative properties of hippocampal CA1 pyramidal neurons. *J. Neurosci.*, **18**, 7613–7624.

Magee, J.C. (1999) Dendritic Ih normalizes temporal summation in hippocampal CA1 neurons. *Nature Neurosci.*, **2**, 508–514.

Mercuri, N.B., Bonci, A., Calabresi, P., Stefani, A. & Bernardi, G. (1995) Properties of the hyperpolarization-activated cation current Ih in rat midbrain dopaminergic neurons. *Eur. J. Neurosci.*, **7**, 462–469.

Moosmang, S., Biel, M., Hofmann, F. & Ludwig, A. (1999) Differential distribution of four hyperpolarization-activated cation channels in mouse brain. *Biol. Chem.*, **380**, 975–980.

Owens, S., Cuttle, M.F., Rusznak, Z. & Forsythe, I. (1999) Pre- and post-synaptic inward rectifier current I (h) in consecutive nuclei in the rat auditory brainstem. *BNA Abstracts*, **15**, 42.05.

Pape, H.C. (1994) Specific bradycardic agents block the hyperpolarization-activated cation current in central neurons. *Neuroscience*, **59**, 363–373.

Pape, H.C. (1996) Queer current and pacemaker: the hyperpolarization-activated cation current in neurons. *Annu. Rev. Physiol.*, **58**, 299–327.

Pape, H.C. & McCormick, D.A. (1989) Noradrenaline and serotonin selectively modulate thalamic burst firing by enhancing a hyperpolarization-activated cation current. *Nature*, **340**, 715–718.

Santoro, B., Grant, S.G., Bartsch, D. & Kandel, E.R. (1997) Interactive cloning with the SH3 domain of N-src identifies a new brain specific ion channel protein, with homology to eag and cyclic nucleotide-gated channels. *Proc. Natl Acad. Sci. USA*, **94**, 14815–14820.

Santoro, B., Liu, D.T., Yao, H., Bartsch, D., Kandel, E.R., Siegelbaum, S.A. & Tibbs, G.R. (1998) Identification of a gene encoding a hyperpolarization-activated pacemaker channel of brain. *Cell*, **93**, 717–729.

Seifert, R., Scholten, A., Gauss, R., Mincheva, A., Lichter, P. & Kaupp, U.B. (1999) Molecular characterization of a slowly gating human hyperpolarization-activated channel predominantly expressed in thalamus, heart, and testis. *Proc. Natl Acad. Sci. USA*, **96**, 9391–9396.

Solomon, J.S. & Nerbonne, J.M. (1993) Two kinetically distinct components of hyperpolarization-activated current in rat superior colliculus-projecting neurons. *J. Physiol. (Lond)*, **469**, 291–313.

Steriade, M. (1998) Corticothalamic networks, oscillations, and plasticity. *Adv. Neurol.*, **77**, 105–134.

Takigawa, T., Alzheimer, C., Quasthoff, S. & Grafe, P. (1998) A special blocker reveals the presence and function of the hyperpolarization-activated cation current IH in peripheral mammalian nerve fibres. *Neuroscience*, **82**, 631–634.

Tkatch, T., Baranauskas, G. & Surmeier, J.D. (1998) Basal forebrain neurons adjacent to the globus pallidus co-express GABAergic and cholinergic marker mRNAs. *Neuroreport*, **9**, 1935–1939.

Tkatch, T., Baranauskas, G. & Surmeier, J.D. (2000) Kv4.2 mRNA abundance and A-type K+ current amplitude are linearly related in basal ganglia and basal forebrain neurons. *J. Neurosci.*, **20**, 579–588.